Characterisation of extensional rheological filament stretching with a dual-mode Giesekus model

Bart Hallmark[1,*], Nicolas Pistre[2] and D. Ian Wilson[1]

[1]Department of Chemical Engineering and Biotechnology, New Museums Site, Pembroke St, Cambridge. CB2 3RA

[2]École Nationale Supérieure de Techniques Avancées, 828 Boulevard des Maréchaux, 91120 Palaiseau, Paris, France.

*Corresponding author: bh206@cam.ac.uk

Abstract

A new, simple, formulation that describes capillary thinning as predicted by a two-mode Giesekus model is derived, and its application in analysing data from extensional rheometry (capillary thinning) experiments is discussed. An algorithm is presented that can be used to fit the expressions obtained from the Giesekus model to extensional rheometry data. Examples of data fitting are given for an idealised data set, for measurements obtained for aqueous solutions of 6 wt% 900,000 molecular weight polyethylene oxide, and for biological fluids obtained from pitchers of *Nepenthes Rafflesiana*. Good fits to the data were obtained, with coefficients of determination in excess of 0.98. For each data set, it was possible to calculate values of extensional viscosity and relaxation time for each of the two modes, allowing quantitative comparison of different fluids or of the same fluid as it ages.

Keywords: Extensional rheometry, Giesekus fluids, multimode viscoelasticity, filament thinning

Introduction

Fluids exhibiting complex rheological response are widespread, with examples ranging from polymer solutions to polymer melts, from emulsions to bubbly liquids, and from dense suspensions to foams. Complex fluids may exhibit viscoelastic behaviour, the effects of which must be taken into account when designing processes to handle them or products that contain them. Many processes will subject a fluid to both shear and extension, hence it is important to understand the fluid's response to these deformations, and also for any modelling done to be able to represent both deformation modes accurately.

Rheometers capable of characterising a complex fluid's shear response have been available for many years, however devices that can accurately characterise a complex fluid's extensional behaviour in isolation are relatively recent[1]. One experimental approach that has been used actively over the past two decades is that of capillary breakup rheometry; the basic principle of this technique is shown in Figure 1. A small cylindrical sample of liquid is loaded between two parallel flat plates, which are then drawn apart rapidly; this causes a liquid filament to form that subsequently reduces in diameter and eventually breaks. Capillary breakup rheometers typically track the mid-filament diameter as a function of time using optical means; photo cells, laser micrometers and high-speed imaging are all approaches that have been used. The liquid filament microrheometer[2], developed by Bazilevsky and co-workers, was able to use fluid samples as small as 0.01 cm^3 and was capable of interrogating the response of fluids with relaxation times as low as 0.01 s. The CaBER™ (Capillary Breakup Extensional Rheometer)[3] was developed by McKinley and co-workers at MIT in the early 2000s in conjunction with the Cambridge Polymer Group; this high-precision instrument uses a laser micrometer to track the mid-filament diameter and is currently the only commercial readily-available extensional rheometer. The Cambridge TriMaster™ [4] was developed by Tuladhar and Mackley at the University of Cambridge in about 2008, and was motivated by the desire to study low viscosity inkjet liquids; this device uses high-speed video imaging and subsequent image analysis to obtain the evolution of mid-filament diameter and is capable of acquiring images roughly every 25 μs[5].

Conventional extensional rheometers, whether bespoke or commercially-available, like most laboratory rheometers are heavy, delicate and expensive. Sometimes it is not possible to test the extensional response of a delicate fluid in a laboratory: for example, if a biological fluid found in a plant in a remote geographic location degrades rapidly it may neither be possible nor economically viable to transport it to a laboratory quickly. To solve this problem, a portable extensional rheometer, named Seymour, was developed at the University of Cambridge in 2014[6]; a photograph of this device is shown in Figure 2. The operation of Seymour differs from most extensional rheometers in that only one of the pistons move, and is actuated by a simple solenoid: this is shown schematically in Figure 3. Recent advances in solid-state high speed cameras, powered by a laptop and capable of up to 500 frames per second yet only having a footprint of one square inch, have allowed high-speed video imaging and image analysis to become a robust and viable method of gathering data in a portable instrument such as Seymour.

The stable and unstable behaviour of capillaries consisting of Newtonian and non-Newtonian fluids has received extensive attention in the literature[7–9], so those aspects are not repeated here. In general, when analysing data obtained from a capillary breakup rheometer, it is usual to present the evolution of the normalised mid-filament diameter, $D(t)/D_0$, as a function of time. A number of analytical expressions have been developed that relate $D(t)/D_0$ to parameters in constitutive models such as viscosity and relaxation time. The fluid's rheology is quantified by selecting a model and fitting the appropriate expression to determine the values of the parameters. Some of the more commonly-used analytical expressions are given in Table 1. Figure 4 shows typical filament thinning profiles for Newtonian, Upper Convected Maxwell (UCM) and Giesekus fluids. All three expressions predict simple filament thinning behaviour, with the rate of change of filament diameter either remaining constant or increasing exponentially with time.

Some complex fluids display extensional responses similar to those shown in Figure 4. However, when contributions from solvent viscosity are significant, or multiple relaxation modes are present,

then the rate of change of filament diameter as a function of time will deviate from these behaviours. Examples of experimental data that exhibit a more complex response are shown in Figure 5(A) for a 6 wt% solution of 900,000 molecular weight PEO in de-ionised water[10] and in Figure 5(B) for fluid extracted from pitchers of *Nepenthes Rafflesiana*[11]. Both of these data sets shown that there is an initial regime where the filament diameter decreases rapidly, followed by a second regime where the change in diameter follows a different kinetic. This effect has been observed in the literature for a number of systems, including solutions of diethyl phthalate[12] and solutions of cellulose in 1-ethyl-3-methylimidazolium acetate[13]. One-dimensional analysis has revealed that this type of response can be attributed to the viscous solvent dominating the early stages of the filament thinning process[14–17]: thereafter, one or more relaxation modes control the subsequent elastic phase of the thinning[14], with viscous behaviour being regained in the limit of capillary breakup as the polymer chains are at the limit of finite extension and are behaving as a solution of rigid rods[14].

The rheological constitutive equations used by workers in this area include FENE-CR[14,17], Oldroyd-B[17], and a combined Giesekus-FENE[16] model. Asymptotic analysis of the FENE-P model[14] identified expressions that can used to estimate rheological parameters such as solvent viscosity, elastic modulus and relaxation times from limiting cases of the early viscous regime, middle elastic regime, and limit of finite extensibility. Two- and three-dimensional modelling of capillary thinning using finite-element methods is also reported extensively in the literature. Yao and co-workers[18] examined the response of a multi-mode Giesekus fluid in extension using the POLYFLOW code. Webster and co-workers used the multi-mode Giesekus constitutive equation, and the Oldroyd and linear PTT constitutive equations with an arbitrary Langrangian-Eulerian formulation to examine the dynamics of filament stretching[19] and step-strain filament stretching[20,21]. Strain hardening fluids in extension have also been modelled using the Giesekus, Oldroyd and linear PTT models by several workers[22,23].

Previous work[6,24] has demonstrated that a single mode Giesekus model can adequately describe the filament thinning behaviour of some experimental systems, including the oft-observed Newtonian-like approach to filament breakup. Despite finite extensibility effects not being explicitly incorporated within the Giesekus model, the extensional viscosity is bounded due to the inclusion of quadratic

stress terms. It seems conceivable, therefore, that some of the more complex filament thinning behaviour can be described by a two-mode Giesekus model. The objectives of the work presented in this paper are therefore twofold: (i) to obtain simple expressions that allow the calculation of filament thinning profiles according to a two-mode Giesekus model, and (ii) to investigate whether it is possible to obtain parameters for the Giesekus constitutive equation using capillary breakup rheometry. It is highly desirable that the resulting data analysis method should be simple enough to be implemented either within a spreadsheet or a simple computer script in a language such as Python or Matlab®. The aim is that it should be able to provide data analysis capability for use with a portable rheometer, such as Seymour, during use in the field.

Theory

Derivation of a simple expression for the extensional filament thinning of a dual-mode Giesekus fluid

The derivation of an expression that describes the filament thinning of a single mode Giesekus fluid has been presented in a previous paper[24]; that derivation followed the approach developed by Entov and Hinch[14]. The analysis presented in this section follows similar lines and starts by considering the total stress tensor, $\boldsymbol{\sigma}$, for the fluid: it is assumed that the total stress is equal to the hydrostatic pressure, p, added to i components of extra stress, $\boldsymbol{\tau}_i$, due to the presence of a polymer

$$\boldsymbol{\sigma} = -p\mathbf{I} + \sum_i \boldsymbol{\tau}_i \tag{1}$$

Each of the i components of extra stress are assumed to be modelled by the Giesekus equation, with the contribution of the viscous solvent being negligible[25]

$$\frac{\boldsymbol{\tau}_i}{\lambda_i} + \frac{\partial \boldsymbol{\tau}_i}{\partial t} + \mathbf{v}\cdot\boldsymbol{\nabla}\boldsymbol{\tau}_i - \left((\boldsymbol{\nabla}\mathbf{v})^{\mathrm{T}}\cdot\boldsymbol{\tau}_i + \boldsymbol{\tau}_i\cdot(\boldsymbol{\nabla}\mathbf{v})\right) = \frac{\eta_{0,i}}{\lambda_i}\dot{\boldsymbol{\gamma}} - \frac{a_i}{\eta_{0,i}}\boldsymbol{\tau}_i\cdot\boldsymbol{\tau}_i$$

(2)

The same assumptions and simplifications that were used previously[24] are applied here, *i.e.* that extensional deformations only occur in the axial and radial directions within the liquid filament, that the dot product of the velocity field and the divergence of the extra stress tensor is zero due to the homogeneity of the flow field (implying that the rate of strain is uniform everywhere in the fluid) and that the axial extensional stress is the dominant stress in the problem. Writing the axial component of Equation (2) for two modes gives:

$$\frac{\tau_{zz,1}}{\lambda_1} + \frac{\partial \tau_{zz,1}}{\partial t} - \tau_{zz,1}\dot{\gamma}_{zz} = \frac{\eta_{0,1}}{\lambda_1}\dot{\gamma}_{zz} - \frac{a_1}{\eta_{0,1}}\tau_{zz,1}^2$$

(3)

$$\frac{\tau_{zz,2}}{\lambda_2} + \frac{\partial \tau_{zz,2}}{\partial t} - \tau_{zz,2}\dot{\gamma}_{zz} = \frac{\eta_{0,2}}{\lambda_2}\dot{\gamma}_{zz} - \frac{a_2}{\eta_{0,2}}\tau_{zz,2}^2$$

(4)

In principle, the inclusion of more than two modes is quite straightforward at this point. The terms on the left and right hand sides of Equations (3) and (4) are now summed and equated *viz*.

$$\frac{\tau_{zz,1}}{\lambda_1} + \frac{\tau_{zz,2}}{\lambda_2} + \frac{\partial}{\partial t}\left(\tau_{zz,1} + \tau_{zz,2}\right) - \dot{\gamma}_{zz}\left(\tau_{zz,1} + \tau_{zz,2}\right) = \dot{\gamma}_{zz}\left(\frac{\eta_{0,1}}{\lambda_1} + \frac{\eta_{0,2}}{\lambda_2}\right) - \frac{a_1}{\eta_{0,1}}\tau_{zz,1}^2 - \frac{a_2}{\eta_{0,2}}\tau_{zz,2}^2$$

(5)

Some terms in Equation (5) can be substituted by considering the force balance in a cylindrical element of fluid and by using Equation (1). The boundary conditions on the liquid filament assume that it is connected to large, stagnant, drops[14] on each of the rheometer plates resulting in zero axial stress. As discussed in a previous paper[24], other boundary conditions that describe the normal stress state of a viscoelastic material have been used by other workers[26] but these are not considered here. The radial stress that causes the filament to thin is assumed to be entirely due to surface tension, α,

and is assumed to be equal to the Laplace pressure. The surface tension is assumed to be constant. These two boundary conditions can be derived from Equation (1) and give

$$\sigma_{zz} = 0 = -p + \sum_i \tau_{zz,i} \tag{6}$$

$$\sigma_{rr} = -\frac{2\alpha}{D} = -p + \sum_i \tau_{rr,i} \tag{7}$$

Substitution of the pressure term from Equation (6) into Equation (7), and the subsequent neglect of radial terms (as before[24]), allows the axial extra stress to be related to the capillary pressure by

$$\sum_i \tau_{zz,i} \approx \frac{2\alpha}{D} \tag{8}$$

The calculation of the time-dependent variation of filament diameter requires an expression that relates the radial and axial extensional rates to the rate of change of filament diameter. It can be shown[24] that this is described by a simple ordinary differential equation in terms of the radial direction extension rate, giving

$$\dot{\gamma}_{zz} = -\frac{4}{D}\frac{\mathrm{d}D}{\mathrm{d}t} \tag{9}$$

The expressions in Equations (9) and (8) can be substituted into Equation (5); some manipulation of the final result gives

$$\frac{\tau_{zz,1}}{\lambda_1} + \frac{\tau_{zz,2}}{\lambda_2} + \frac{6\alpha}{D^2}\frac{\mathrm{d}D}{\mathrm{d}t} = -\frac{4}{D}\frac{\mathrm{d}D}{\mathrm{d}t}\left(\frac{\eta_{0,1}}{\lambda_1} + \frac{\eta_{0,2}}{\lambda_2}\right) - \frac{a_1}{\eta_{0,1}}\tau_{zz,1}^2 - \frac{a_2}{\eta_{0,2}}\tau_{zz,2}^2$$

(10)

Further rearrangement of Equation (10) yields an ordinary differential equation that relates the rate of change of filament diameter to the Giesekus parameters for each of the two modes, and to the axial extra stress due to each of the two modes in Equation (2).

$$\frac{\mathrm{d}D}{\mathrm{d}t} = \frac{-\lambda_1\lambda_2\left(a_1\eta_{0,2}\tau_{zz,1}^2 + a_2\eta_{0,1}\tau_{zz,2}^2\right) - \eta_{0,1}\eta_{0,2}\left(\lambda_2\tau_{zz,1} + \lambda_1\tau_{zz,2}\right)}{\eta_{0,1}\eta_{0,2}\lambda_1\lambda_2\left(\frac{6\alpha}{D^2} + \frac{4}{D}\left(\frac{\lambda_2\eta_{0,1+}\lambda_1\eta_{0,2}}{\lambda_1\lambda_2}\right)\right)}$$

(11)

If the two modes of the fluid are identical, *i.e.* they have the same relaxation times, zero shear rate viscosities and mobility parameters, then Equation (11) should reduce to the expression that has been previously derived[24] to describe the filament thinning of a single mode Giesekus fluid. Under these conditions, the total axial extra stress will consist of equal extra stress contributions from each mode, *viz*.

$$\frac{\tau_{zz}}{2} = \tau_{zz,1} = \tau_{zz,2}$$

(12)

The mechanical response of the two-mode fluid filament should match that of the single mode fluid, but each of the two modes is subject to half the stress. As a thought experiment, if this situation were applied to the phenomenological Maxwell element[27], then the element's mechanical response is preserved if the spring modulus, g, and damper viscosity, η, are both halved, *i.e.*

$$g_1 = g_2 = \frac{g}{2}$$

(13)

$$\eta_1 = \eta_2 = \frac{\eta}{2}$$

(14)

The relaxation time, λ, is defined as $\lambda = \frac{\eta}{g}$; this should hence remain unscaled. Referring back to the Giesekus fluid, it will be assumed for this particular case that the level of non-linearity in the system due to the mobility parameter, *a*, is the same for each mode, *i.e.*

$$a_1 = a_2 = a \tag{15}$$

Substitution of Equations (14) and (15) into Equation (11) yields, after some rearrangement,

$$\frac{\mathrm{d}D}{\mathrm{d}t} = -\frac{a{\tau_{zz}}^2\lambda - \tau_{zz}\eta_0}{\eta_0\lambda\left(\frac{6\alpha}{D^2} + \frac{4}{D}\left(\frac{\eta_0}{\lambda}\right)\right)} \tag{16}$$

Remembering that $\tau_{zz} \approx \frac{2\alpha}{D}$ and substituting this into Equation (16) gives the result obtained previously for a single mode fluid[24], namely

$$\frac{\mathrm{d}D}{\mathrm{d}t} = \frac{-\alpha}{\eta_0}\left(\frac{\eta_0 D + 2\alpha a\lambda}{2\eta_0 D + 3\alpha\lambda}\right) \tag{17}$$

Developing a solution algorithm

Inspection of Equation (11) shows that the rate of change of filament diameter is dependent on the fluid's material properties (zero shear rate viscosity, mobility parameter and relaxation time), the filament diameter, *D*, and the axial extra stress present in each mode, $\tau_{zz,i}$. An expression for the rate of change of axial extra stress can be obtained by combining Equation (3), or Equation (4), with Equation (9), *viz*

$$\frac{\mathrm{d}\tau_{zz,i}}{\mathrm{d}t} = \frac{-\tau_{zz,i}}{\lambda_i} - \frac{a_i}{\eta_{0,i}}\tau_{zz,i}^2 - \frac{4}{D}\frac{\mathrm{d}D}{\mathrm{d}t}\left(\frac{\eta_{0,i}}{\lambda_i} + \tau_{zz,i}\right)$$

(18)

It can be seen that Equation (18) is coupled to Equation (11) and they must be solved simultaneously.

In order to solve Equation (11) to predict filament thinning, the distribution of the total axial extra stress between the two modes needs to be known and, at the start of the filament thinning process at time $t = 0$, an initial stress condition is required in order to start the calculation. The original FENE-P model derived by Entov and Hinch[14] assumed that the viscoelastic stress at the end of the initial filament stretch was zero; this was later refined when comparison was made to experimental data[28] to allow an initial viscoelastic stress to be present. Anna and McKinley[7] discussed the selection of the initial viscoelastic stress condition in some detail, identifying that the fluid filament starts to stretch at a rate that prevents the longest mode relaxing. Clasen and co-workers[29] also identified this initial condition, but then note that the extension rates produced by the early stages of filament thinning are insufficient to the keep the longest mode stretched and that the initial viscoelastic stress decays rapidly. Once filament thinning progresses, it is understood that the polymer coils become extended once again[29].

A simplifying assumption has been made in this work: the stress contribution from the initial filament stretch has been neglected, after the initial FENE-P model of Entov and Hinch[14], but the stress due to the capillary force balance is distributed across the two modes in the inverse proportion to the ratio of the relaxation times. Physically, this implies that the initial stress state within the fluid at the start of filament thinning is dominated by the mode that is able to adapt fastest to the initial extension rates. This assumption is also related to that made by Wagner and co-workers[15] in their consideration of the filament thinning of a dilute polymer solution in a Newtonian solvent: they assumed that the early stages of filament thinning are dominated by the solvent dynamics since the polymer will not have had time to respond to the applied deformation, and is hence unable to contribute to the stress.

This initial extra stress condition allows an initial value of $\frac{\mathrm{d}D}{\mathrm{d}t}$ to be calculated which, in turn, allows Equation (18) to be solved; this requires use of the same initial condition. Solving Equation (18)

yields the rate of change of extra stress for each mode, $\frac{\mathrm{d}\tau_{zz,i}}{\mathrm{d}t}$, which allows the extra stress distribution for the next time step, at time $t > 0$, to be calculated. Direct use of the result from Equation (18) to calculate the extra stress distribution will not be made, rather it will be used as a predictor of the ratio of the extra stresses between the two modes, with the total extra stress being calculated using Equation (8) with the new filament diameter resulting from Equation (11).

The solution procedure can therefore be written as:

1. Assume a set of relaxation times, mobility parameters and zero shear rate viscosities for both modes. Choose a time-step, δt, that is based on the frame-rate of the experimental data.
2. At time $t = 0$, the filament diameter $D = D_0$. Use of Equation (8), $\tau_{zz,1} + \tau_{zz,2} = \tau_{zz} \approx \frac{2\alpha}{D}$, allows the extra axial stress, τ_{zz}, to be evaluated.
3. Assume that $\tau_{zz,1} = \frac{\lambda_2}{\lambda_1+\lambda_2}\tau_{zz}$ and that $\tau_{zz,2} = \tau_{zz} - \tau_{zz,1}$.
4. Use Equation (11) to calculate $\frac{\mathrm{d}D}{\mathrm{d}t}$. For an assumed time-step, δt, calculate the new filament diameter, D, at the next time step by $D(t + \delta t) = D(t) + \frac{\mathrm{d}D}{\mathrm{d}t}\delta t$.
5. Use $\frac{\mathrm{d}D}{\mathrm{d}t}$ in Equation (18) to calculate a prediction of the new extra stress, $\tau^*_{zz,i}$, due to each mode, *viz:*

$$\tau^*_{zz,i}(t + \delta t) = \tau_{zz,i}(t) + \frac{\mathrm{d}\tau_{zz,i}}{\mathrm{d}t}\delta t$$

6. Use the predicted extra stress for each mode to calculate a corrected extra stress from the Laplace pressure *via* Equation (8):

$$\tau_{zz,1}(t + \delta t) = \frac{\tau^*_{zz,1}(t + \delta t)}{\tau^*_{zz,1}(t + \delta t) + \tau^*_{zz,2}(t + \delta t)}\frac{2\alpha}{D(t + \delta t)}$$

$$\tau_{zz,2}(t + \delta t) = \frac{\tau^*_{zz,2}(t + \delta t)}{\tau^*_{zz,1}(t + \delta t) + \tau^*_{zz,2}(t + \delta t)}\frac{2\alpha}{D(t + \delta t)}$$

7. Repeat from step (4) for $t = t + \delta t$.

This solution procedure is straightforward to implement in a spreadsheet or programming language such as Matlab® or Python. If the intention is to obtain material parameters from a set of extensional rheometry data, then the material properties used in step (1) will require initial estimation and subsequent optimisation using a suitably chosen objective function. This is considered in the next section. In order to generate initial estimates of the material parameters, however, it would be useful to understand how their variation affects the form of the predicted filament thinning profile. This is considered first.

Discussion

Equation (11) has six adjustable parameters that describe the filament thinning process for a dual-mode Giesekus fluid; a set of three for the short relaxation mode (smaller value of λ) and a set of three for the long relaxation mode (larger value of λ). In order to explore the effect of systematic variation of the parameters on each mode on the form of the predicted filament thinning profile, an arbitrary set of parameters has been defined as given in Table 2Table 1; this is used as a datum. The solution to Equation (11) using these parameters is shown by the bold black line in Figure 6. In this Figure it can be seen that the dual-mode formulation successfully captures the initial region of filament decay that was seen in the experimental data for both PEO in Figure 5(A) and for the pitcher plant fluids in Figure 5(B).

Figure 6 also shows the effect of varying the short mode parameters, $\eta_{0,2}$, a_2 and λ_2, on the reduction in normalised filament diameter, D/D_0, as a function of non-dimensional time, t/λ_1; the long mode parameters were held constant at their datum values. Detailed examination of Figure 6 shows that increasing the zero shear rate viscosity, $\eta_{0,2}$, from $0.005\eta_{0,1}$ to $0.03\eta_{0,1}$, as shown by the light grey lines, has a qualitatively very similar effect to decreasing the mobility parameter, a_2, from being equal to a_1 to $0.1a_1$, as shown by the dashed and dotted lines. Variation of these two parameters decreases the initial rate of change of normalised filament diameter, D/D_0, over the range $0 < t/\lambda_1 < 0.1$. Furthermore, the time taken for the normalised filament diameter, D/D_0, to reach a value of 0.01

increases from about $t/\lambda_1 = 0.62$ to about $t/\lambda_1 = 0.90$; it is notable that the shape of the D/D_0 curves appear to be similar. The inset in Figure 6 illustrates the impact of increasing λ_2 from $0.05\lambda_1$ to $0.2\ \lambda_1$: as its value approaches that of λ_1 the initial gradient of D/D_0 remains essentially unchanged but the magnitude of the reduction of D/D_0 in the region of initial filament decay decreases. The time for D/D_0 to reach a value of 0.01 also increases significantly from about $t/\lambda_1 = 0.62$ to about $t/\lambda_1 = 1.1$.

The plot shown in Figure 7 shows the reverse scenario: the short mode parameters are held at their datum values whilst the long mode parameters, $\eta_{0,1}$, a_1 and λ_1, are systematically varied. In this plot, time has again been non-dimensionalised by λ_1. It can be seen in this plot that there is striking similarity between the effect of decreasing $\eta_{0,1}$ from $200\,\eta_{0,2}$ to $20\,\eta_{0,2}$ and the effect of increasing a_1 from being equal to a_2 to being $10a_2$. Alteration of both of these parameters has no significant effect on either the initial rate of change of D/D_0 or the magnitude of its reduction: D/D_0 reaches a value of approximately 0.24 by $t/\lambda_1 = 0.02$. The significant effect is that the time taken for D/D_0 to reach a value of 0.01 decreases from about $t/\lambda_1 = 0.62$ to about $t/\lambda_1 = 0.075$. The inset in Figure 7 illustrates the impact of decreasing λ_1 from $20\lambda_2$ to $2\lambda_2$: the initial rate of change of D/D_0, and the magnitude of its reduction, are both significantly reduced. In the case where $\lambda_1 = 2\lambda_2$, as shown by the dotted line, the initial region becomes essentially negligible and the form of the filament thinning profile approaches that of a single-mode Giesekus fluid.

The similarity of the filament thinning profiles that are obtained when independently varying a and η_0 at constant λ for the same mode warrants further consideration. Interestingly, the ratio of these terms feature in the definition of the extensional viscosity for the Giesekus model. For a uniaxial deformation, it can been shown that the steady-state extensional viscosity at high strain rate is $2\eta_0/a$ [30]. To assist clarity and insight, three groups of parameters are defined, namely

$$\eta_{E,1} = \frac{2\eta_{0,1}}{a_1} \tag{19}$$

$$\eta_{E,2} = \frac{2\eta_{0,2}}{a_2} \tag{20}$$

$$\theta = \frac{\eta_{0,1}}{\eta_{0,2}} \tag{21}$$

If the groups defined in Equations (19) to (21) are substituted into Equation (11), one obtains, after some manipulation

$$\frac{\mathrm{d}D}{\mathrm{d}t} = -\frac{D^2\left(\lambda_1\tau_{zz,2} + \lambda_2\left(\tau_{zz,1} + {2\lambda_1\tau_{zz,1}^2}\Big/{\eta_{E,1}} + {2\lambda_1\tau_{zz,2}^2}\Big/{\eta_{E,2}}\right)\right)}{6\alpha\lambda_1\lambda_2 + 4D\eta_{0,2}(\lambda_1 + \theta\lambda_2)} \tag{22}$$

If the term containing D in the denominator is $\ll 6\alpha\lambda_1\lambda_2$, this gives

$$\frac{\mathrm{d}D}{\mathrm{d}t} \approx -\frac{D^2\left(\lambda_1\tau_{zz,2} + \lambda_2\left(\tau_{zz,1} + {2\lambda_1\tau_{zz,1}^2}\Big/{\eta_{E,1}} + {2\lambda_1\tau_{zz,2}^2}\Big/{\eta_{E,2}}\right)\right)}{6\alpha\lambda_1\lambda_2} \tag{23}$$

Equation (23) shows that the extensional viscosities, $\eta_{E,1}$ and $\eta_{E,2}$, control the filament thinning as opposed to unique values of a and η_0; this is an important result. If Equation (11) is being fitted to experimental data, it will be necessary to specify either a or η_0 from an estimate and then to optimise the remaining parameters to obtain the best fit possible.

Insight into the filament behaviour near filament break-up can be obtained by assuming that the extra stress due to the long relaxation mode dominates. If the extra stress resulting from the capillary

pressure is distributed between the two modes according to Equation (8), then $\tau_{zz,1} = {2\alpha(1-\varphi)}/{D}$ and $\tau_{zz,2} = {2\alpha\varphi}/{D}$. Here, φ is a parameter that quantifies the stress distribution between the two modes and when $\tau_{zz,1} \gg \tau_{zz,2}$, $\varphi \to 0$. If these extra stress expressions are substituted into Equation (11), along with the groups defined in Equations (19) to (21), one obtains

$$\frac{\mathrm{d}D}{\mathrm{d}t} \approx -\frac{\left(\varphi D\lambda_1 + \lambda_2\left((1-\varphi)D + {\lambda_1 4\alpha(1-\varphi)^2}/{\eta_{E,1}} + {\lambda_1 4\alpha\varphi^2}/{\eta_{E,2}}\right)\right)}{3\lambda_1\lambda_2} \tag{24}$$

In the limit of small diameter, and as $\varphi \to 0$, Equation (24) yields

$$\frac{\mathrm{d}D}{\mathrm{d}t} \approx -\frac{4\alpha}{3\eta_{E,1}} \tag{25}$$

Equation (25) shows that as the filament approaches breakup, the rate of diameter change is entirely governed by the extensional viscosity of the long relaxation mode and by surface tension. This observation further reinforces the need to have a reliable heuristic to specify either a_1 or $\eta_{0,1}$ prior to fitting Equation (11) to experimental data such that an initial estimate of $\eta_{E,1}$ can be obtained.

Equation (24) can also be used to deduce an analytical expression for the filament diameter when $\tau_{zz,1} \gg \tau_{zz,2}$. Integrating Equation (24) from the lower bound that marks the end of the initial rate of change of normalised filament diameter, designated t_H and D_H for time and filament diameter respectively, yields

$$\int_{t_H}^{t} \mathrm{d}t = \int_{D_H}^{D} -\frac{3\lambda_1\lambda_2\eta_{E,1}\eta_{E,2}}{\left(\eta_{E,1}\eta_{E,2}(\varphi\lambda_1 + (1-\varphi)\lambda_2)D + 4\alpha\lambda_1\lambda_2\left(\eta_{E,2}(1-\varphi)^2 + \eta_{E,1}\varphi^2\right)\right)}\mathrm{d}D$$

$$\Rightarrow \frac{t}{\lambda_1} = \frac{t_H}{\lambda_1} - \frac{3\lambda_2}{(\varphi\lambda_1 + (1-\varphi)\lambda_2)} \left(\ln \left[\frac{\eta_{E,1}\eta_{E,2}(\varphi\lambda_1 + (1-\varphi)\lambda_2)\, {}^{D}/_{D_H} + 4\alpha\lambda_1\lambda_2\left(\eta_{E,2}(1-\varphi)^2 + \eta_{E,1}\varphi^2\right)/_{D_H}}{\eta_{E,1}\eta_{E,2}(\varphi\lambda_1 + (1-\varphi)\lambda_2) + 4\alpha\lambda_1\lambda_2\left(\eta_{E,2}(1-\varphi)^2 + \eta_{E,1}\varphi^2\right)/_{D_H}} \right] \right)$$

(26)

A comparison between the numerical solution of Equation (11), using parameters from Table 1, and the analytical solution of Equation (26) is shown in Figure 8 for the case where $\varphi \to 0$. A value of ${}^{t_H}/_{\lambda_1}$ was chosen such that the coefficient of determination[31], R^2, comparing the predictions of Equation (11) and Equation (26) over the second regime of filament thinning just exceeded 0.99. This resulted in ${}^{D_H}/_{D_0} = 0.265$ and ${}^{t_H}/_{\lambda_1} = 0.031$. Examination of the filament thinning profile in Figure 8 shows that these values of ${}^{D_H}/_{D_0}$ and ${}^{t_H}/_{\lambda_1}$ do indeed demarcate the two filament thinning regimes. It is noteworthy that Equation (26) is implicit with respect to ${}^{D}/_{D_H}$ but explicit in terms of ${}^{t}/_{\lambda_1}$, hence ${}^{t}/_{\lambda_1}$ is solved as a function of ${}^{D}/_{D_H}$ as opposed to *vice-versa*. It can be seen from Figure 8 that Equation (26) captures the long relaxation mode behaviour quite well, including the approach to filament break up, but does not capture the initial regime of filament thinning. This is not surprising since the contribution of the short relaxation mode to the extra stress has been neglected.

An estimate of the non-dimensional filament rupture time, ${}^{t_F}/_{\lambda_1}$, can be obtained from Equation (26) by examining the limit where ${}^{D}/_{D_H}$ and φ tend to zero, *viz*:

$${}^{t_F}/_{\lambda_1} = {}^{t_H}/_{\lambda_1} + 3\left(\ln \left[{}^{\eta_{E,1}D_H}/_{4\alpha\lambda_1} + 1 \right] \right)$$

(27)

Substitution of the parameters in Table 1 into Equation (27) along with ${}^{D_H}/_{D_0} = 0.265$ and ${}^{t_H}/_{\lambda_1} = 0.031$ gives ${}^{t_F}/_{\lambda_1} = 0.065$; numerical solution of Equation (11) shows that ${}^{t}/_{\lambda_1} = 0.065$ when ${}^{D}/_{D_H} = 0$. Equation (27) demonstrates again that the approach to filament break-up is governed

essentially entirely by the long relaxation mode, with the long mode extensional viscosity being an important parameter; Equation (27) hence provides a method to estimate $\eta_{E,1}$, and hence a_1, given $\eta_{0,1}$, λ_1, D_H and α.

Fitting experimental data

The objective when developing Equation (11) was to be able to obtain parameters for the long and short modes of the Giesekus equation from extensional rheometry data alone. The discussion above has highlighted that the long and short mode extensional viscosities, written as quotients of zero shear rate viscosity and mobility parameter, are partly responsible for controlling the filament thinning process. When fitting Equation (11) to experimental data using an iterative algorithm, it will be important to choose reasonable values of either the mobility parameter or the zero shear rate viscosity as initial conditions for both modes. The remaining parameter for each mode, along with the relaxation times for both modes, will then need estimation such that minimisation of a suitably-chosen objective function will be able to provide the best correlation between Equation (11) and experimental data. This is explored in more depth next.

Fitting idealised data – impact of initial conditions and choice of objective function

A number of expressions that relate D/D_0 to t were presented in Table 1. It can be seen that the Newtonian expression can be used to calculate a characteristic viscosity, and that the UCM expression can be used to calculate a characteristic relaxation time. Fitting the Newtonian and UCM expressions to different ranges of the experimental data, namely the initial region of filament thinning and the second regime of filament thinning, will give initial estimates for Giesekus parameters $\eta_{0,1}$, $\eta_{0,2}$, λ_1 and λ_2; an example of one way these two equations can be fitted to data is shown in Figure 9(A). The data shown in this plot are idealised data and have been obtained by solving Equation (11) with the parameters given in Table 3; testing the fitting procedure on idealised data allows comparison between the parameters used to generate the data and parameters resulting from the data fitting.

Estimates of the initial parameters were obtained as illustrated in Figure 9(A): $\eta_{0,1}$ was obtained by fitting the Newtonian expression in Table 1 to the filament break up time, $\eta_{0,2}$ by the best fit of the

Newtonian expression (by use of the coefficient of determination[31], R^2) to the initial region of filament thinning, λ_1 by fitting the UCM expression such that it is the best fit to the second regime of filament thinning and λ_2 by fitting the UCM expression such that it is a best fit to the initial regime of filament thinning. The time and filament diameter at the end of the initial region of filament decay, t_H and D_H, along with an approximate time for filament breakup, t_F, can then be estimated from the idealised data. These data can then be used to estimate $\eta_{E,1}$, hence a_1, by rearrangement of Equation (27)

$$\eta_{E,1} = \frac{4\alpha\lambda_1 \exp\left(\frac{t - t_H}{3\lambda_1}\right) - 1}{D_H} \tag{28}$$

The only unknown parameter remaining is a_2. In the first instance, this will be assumed to be the same as a_1; the initial set of parameters is given in Table 3**.**

The choice of objective function used to fit the prediction of Equation (11) to the idealised data is important as the range of ${}^{D}/_{D_0}$ typically spans a minimum of two decades. A number of approaches to minimise the error between predicted values and idealised data were tested, but it was found that an objective function based on one of the formulations of the coefficient of determination, R^2, denoted as R_1^2 in the review by Kvålseth[31], was most robust. Kvålseth[31] defined R_1^2 as

$$R_1^2 = 1 - \frac{\sum_j \left(\left({}^{D}/_{D_0}\right)_{j,m} - \left({}^{D}/_{D_0}\right)_{j,p} \right)^2}{\sum_j \left(\left({}^{D}/_{D_0}\right)_{j,m} - \left(\overline{{}^{D}/_{D_0}}\right)_{m} \right)^2} \tag{29}$$

Here, subscript 'm' denotes measured values, subscript 'p' denotes predicted values and an overbar denotes an arithmetic mean. The numerator of Equation (29) is the only term that contains the predicted values of ${}^{D}/_{D_0}$, hence minimisation of this will result in the best value of R_1^2. The chosen objective function, ϕ, takes the difference between logarithms of the measured and predicted values of ${}^{D}/_{D_0}$ such that data over the entire two decade range is able to influence the objective function:

$$\phi = \sum_j \left(\ln\left({}^{D_{j,m}}\!/_{D_{j,p}} \right) \right)^2$$

(30)

Figure 9(B) compares the idealised data, generated using the parameters in row 1 of Table 3, and the prediction of Equation (11) using the solution procedure given above: this results in the parameters given in row 3 of Table 3. The objective function, ϕ, was minimised by adjusting a_1, a_2, λ_1 and λ_2: minimisation was performed in Microsoft Excel™ 2013 in three steps. Firstly the generalised reduced gradient algorithm (GRG2[32,33]) was used, with central derivatives and a convergence tolerance set to 1×10^{-8}. This solver is able to minimise smooth non-linear functions, but may not find a global minimum. Secondly the Evolutionary solver[34], a genetic algorithm capable of minimising non-smooth, non-linear functions, was used with its default settings and the 'Random seed' value set to 2 to test whether or not another minima existed. If this second step found a lower value of ϕ, then the GRG2 algorithm was run again to find the exact values of a_1, a_2, λ_1 and λ_2 that defined the new minima. The mobility parameters were constrained to lie between values of 0 and 0.5, since this bounds their region of validity[35,36]. Reasonable upper and lower bounds, of 5 s and 1 ms respectively, were defined for the relaxation times to prevent the minimisation algorithms setting them to either zero or infinity.

The first run of the GRG2 solver took 1 iteration to find a local minimum (with R_1^2 = -6.13), the Evolutionary solver then took 854 iterations to find a point in the solution space where R_1^2 = 0.890 and the final run of the GRG2 solver took a further 271 iterations to reach a solution where R_1^2 = 1.000; the fitted parameters are reported in Table 3. If these parameters are compared to those used to generate the data it can be seen that, as expected, the absolute values of a and η_0 do not match but that the extensional viscosities, $\eta_{E,1}$ and $\eta_{E,2}$, lie within the set precision. Moreover, the values of λ_1 and λ_2 obtained by fitting lie within 2% of the generating ones. It should be noted that the solution procedure outlined above does not force λ_1 to be the long mode and λ_2 to be the short mode, as demonstrated by the fitted values reported in Table 3. These results demonstrate that the data fitting

procedure outlined above is capable of extracting representative values of the relaxation time and extensional viscosity for each mode of Equation (11) from extensional rheometry data.

Fitting experimental data

The data fitting procedure described above was tested on experimental data for a solution of 6 wt% PEO (900,000 molecular weight)[10] and fluid from the same pitcher of *N. Rafflesiana* 3 days and 7 days after opening[11]; the filament thinning profiles of these three fluids were shown in Figure 5. The surface tension of the PEO solution was set to be 63 mN/m, replicating the value measured by Tirtaatmadja and co-workers[37]. The surface tension of the pitcher fluid was assumed to be 72 mN/m; the surface tension of the particular pitchers tested as part of the field trial[6] is unknown, and this represents a potentially large source of error in the rheological parameters reported in Table 4.

In all cases, a good fit was achieved, typically with $R_1^2 > 0.98$. Gauri and Koelling[38] reported that PEO solutions exhibit Giesekus behaviour in extension, and that a single mode Giesekus model could predict the observed filament profile on a fibre-spinning line[39]. Previous work[6] has also identified that a single mode Giesekus model can predict the filament thinning of some pitcher fluid samples. Figure 10 shows the locus of points corresponding to the solution of Equation (11) with parameters given in Table 4 alongside the experimental data.

Examination of the parameters in Table 4 reveals that the long mode extensional viscosity, $\eta_{E,1}$, and the relaxation time, λ_1, differ by an order of magnitude when comparing the PEO solution to the two pitcher plant samples. Furthermore, it can be seen that $\lambda_1 = 5.0$ s for the PEO solution, which was the specified upper bound on relaxation time; it was found that the optimal solution was always found when λ_1 reached the upper bound value, regardless of physical significance. The values of extensional viscosity for both modes, however, remained very similar.

When the parameters for the two pitcher plant samples are compared, it can be seen that they are similar; λ_1 and λ_2 decrease with sample age while $\eta_{E,1}$ and $\eta_{E,2}$ increase with sample age. The increase in $\eta_{E,1}$ and $\eta_{E,2}$ with sample age is surprising and warrants further analysis. The inset graph

in Figure 10(B) plots values of D/D_0 close to filament break-up on linear axes; Equation (**25**) shows that $\eta_{E,1}$ close to filament breakup should be inversely proportional to the gradient of the filament break-up curve, inferring that the final stage of filament thinning is essentially Newtonian. Fitting a linear relationship to the data in the inset graph (not shown in Figure 10(B) for reasons of clarity) demonstrates that the gradient of the two sets of data sets similar: -0.229 1/s with R_1^2 = 0.948 for day 3 and -0.212 1/s with R_1^2 = 0.921 day 7. The low values of R_1^2, coupled with the stepped nature of the experimental data, casts significant doubt on the observed increase in $\eta_{E,1}$ and $\eta_{E,2}$ with sample age. It is likely that this increase is an artefact of fitting Equation (11) over two decades of data, where the level of noise in the data increases with decreasing D/D_0. A further assumption that may affect the values of $\eta_{E,1}$ and $\eta_{E,2}$ is that surface tension remains constant throughout the ageing process.

The similarity of the two parameter sets indicates that the solution algorithm is functioning robustly since the filament thinning curves for these fluids shown in Figure 10(B) are also similar. Anecdotally, this result is of interest since the pitcher plant literature suggests that pitcher fluid relaxation times decrease with time[6] after the opening of a pitcher; however, previous studies have only been able to measure an overall relaxation time. More analysis of pitcher fluid data, along with determination of a representative value for surface tension, is required to examine whether or not this observation applies to both the short and long relaxation modes presented here and as to whether the initial regime of filament thinning correlates to a physiological requirement of the pitcher plant. This is the subject of ongoing work.

Conclusions

A simple method is presented describing how to obtain relaxation times and extensional viscosities for a dual-mode Giesekus fluid undergoing filament stretching. It is, however, not possible to calculate unique values for all six Giesekus parameters for the two modes from the expressions. Despite this limitation, the method presented here allows the relative differences between fluids or samples to be quantified, for example as a biological fluid ages or as a fluid pH is changed.

Fitting experimental data to the expressions developed in this paper requires use of a non-linear optimisation algorithm with a suitably-chosen objective function. Successful data fitting was obtained to a model data set and to experimental data using both the generalised reduced gradient algorithm (GRG2) and the Evolutionary algorithm in Microsoft Excel™ minimising an objective function inspired by the coefficient of determination. A coefficient of determination (R_1^2) value of 1.000 was obtained when fitting the model data set, while R_1^2 values > 0.98 were obtained when fitting extensional rheometry data for a 6 wt% solution of 900k MW polyethylene oxide (PEO) in deionised water and fluids from a pitcher of *N. Rafflesiana*.

Acknowledgements

The authors are grateful to Dr Ulrike Bauer, University of Bristol, for access to experimental data on pitcher plant fluids obtained in the field in Brunei Darussalam between August and September 2014. The authors wish to acknowledge Edward Bosson and Tom Hoier for their data analysis of pitcher plant fluids that identified the initial region of filament thinning, colloquially termed the 'hockey stick'. The authors would also like to acknowledge the highly constructive input from the reviewers.

List of symbols

Roman letters

a	-	Giesekus mobility parameter	(-)
b	-	FENE-P finite extensibility parameter	(-)
D	-	Filament diameter	(m)
D_0	-	Initial filament diameter	(m)
D_p	-	Piston diameter	(m)
E_c	-	Elasto-capillary number	(-)
g	-	Elastic modulus	(Pa)
h_0	-	Initial gap size	(m)
$\mathbf{I}$	-	Identity tensor	(-)
R^2	-	Coefficient of determination	(-)
p	-	Hydrostatic pressure	(Pa)
t	-	Time	(s)
t'	-	Dimensionless time	(-)
$\mathbf{v}$	-	Velocity vector	(m/s)
X	-	Shape factor	(-)

Greek letters

α	-	Surface tension	(N/m)
δt	-	Time step	(s)

φ	-	Stress distribution parameter	(-)
ϕ	-	Objective function to minimise	(-)
$\dot{\boldsymbol{\gamma}}$	-	Strain rate tensor	(1/s)
η	-	Maxwellian damper viscosity	(Pa s)
η_0	-	Zero shear rate viscosity	(Pa s)
η_E	-	Extensional viscosity	(Pa s)
θ	-	Viscosity ratio, $\frac{\eta_{0,1}}{\eta_{0,2}}$	(-)
λ	-	Relaxation time	(s)
$\boldsymbol{\sigma}$	-	Total stress tensor	(Pa)
$\boldsymbol{\tau}$	-	Extra stress tensor	(Pa)
ξ	-	FENE-P dimensionless diameter	(-)

Subscripts

1	-	Long relaxation mode
2	-	Short relaxation mode
F	-	Value at filament breakup
H	-	End of the initial regime of filament thinning
i	-	i^{th} relaxation mode
m	-	Measured value
p	-	Predicted value

rr - Radial component

zz - Axial component

Superscripts

* - Projected value

References

1. Galindo-Rosales FJ, Alves MA, Oliveira MSN. Microdevices for extensional rheometry of low viscosity elastic liquids: a review. *Microfluidics and Nanofluidics*. 2012;14(1-2):1-19.

2. Bazilevsky AV, Entov VM, Rozhkov AN. Liquid filament microrheometer and some of its applications. In: Oliver DR, ed. *Third European Rheology Conference and Golden Jubilee Meeting of the British Society of Rheology*. Dordrecht: Springer Netherlands; 1990:41-43.

3. McKinley GH, Tripathi A. How to extract the Newtonian viscosity from capillary breakup measurements in a filament rheometer. *Journal of Rheology*. 2000;44(3):653.

4. Tuladhar TR, Mackley MR. Filament stretching rheometry and break-up behaviour of low viscosity polymer solutions and inkjet fluids. *Journal of Non-Newtonian Fluid Mechanics*. 2008;148(1-3):97-108.

5. Vadillo DC, Hoath SD, Hsiao W-K, Mackley MR. The effect of inkjet ink composition on rheology and jetting behaviour. In: *Proceedings of the 27th international conference on digital printing technologies, NIP27*. Minneapolis, MN, USA; 2011.

6. Collett C, Ardron A, Bauer U, et al. A portable extensional rheometer for measuring the viscoelasticity of pitcher plant and other sticky liquids in the field. *Plant Methods*. 2015;11(1):16.

7. Anna SL, McKinley GH. Elasto-capillary thinning and breakup of model elastic liquids. *Journal of Rheology*. 2001;45(1):115.

8. Rodd LE, Scott TP, Cooper-White JJ, McKinley GH. Capillary break-up rheometry of low-viscosity elastic fluids. *Applied Rheology*. 2005;15(1):12-27.

9. McKinley GH. Visco-Elasto-Capillary thinning and break-up of complex fluids. *Rheology Reviews*. 2005:1-48.

10. Pistre N. *Private communication*.; 2015.

11. Bauer U. *Private communication*.; 2014.

12. Vadillo DC, Tembley M, Morrison NF, Harlen OG, Mackley MR, Soucemarianadin A. The matching of polymer solution fast filament stretching, relaxation, and break up experimental results with 1D and 2D numerical viscoelastic simulation. *Journal of Rheology*. 2012;56(6):1491.

13. Haward SJ, Sharma V, Butts CP, McKinley GH, Rahatekar SS. Shear and extensional rheology of cellulose/ionic liquid solutions. *Biomacromolecules*. 2012;13(5):1688-99.

14. Entov VM, Hinch EJ. Effect of a spectrum of relaxation times on the capillary thinning of a filament of elastic liquid. *Journal of Non-Newtonian Fluid Mechanics*. 1997;72(1):31-53.

15. Wagner C, Bourouiba L, McKinley GH. An analytic solution for capillary thinning and breakup of FENE-P fluids. *Journal of Non-Newtonian Fluid Mechanics*. 2015;218:53-61.

16. Fontelos MA, Li J. On the evolution and rupture of filaments in Giesekus and FENE models. *Journal of Non-Newtonian Fluid Mechanics*. 2004;118(1):1-16.

17. Tembley M, Vadillo D, Mackley MR, Soucemarianadin A. The matching of a "one-dimensional" numerical simulation and experiment results for low viscosity Newtonian and non-Newtonian fluids during fast filament stretching and subsequent break-up. *Journal of Rheology*. 2012;56(1):159.

18. Yao M, McKinley GH, Debbaut B. Extensional deformation, stress relaxation and necking failure of viscoelastic filaments. *Journal of Non-Newtonian Fluid Mechanics*. 1998;79(2-3):469-501.

19. Matallah H, Sujatha KS, Banaai MJ, Webster MF. Single and multi-mode modelling for filament stretching flows. *Journal of Non-Newtonian Fluid Mechanics*. 2007;146(1-3):92-113.

20. Sujatha KS, Matallah H, Banaai MJ, Webster MF. Modeling step-strain filament-stretching (CaBER-type) using ALE techniques. *Journal of Non-Newtonian Fluid Mechanics*. 2008;148(1-3):109-121.

21. Webster MF, Matallah H, Sujatha KS, Banaai MJ. Numerical modelling of step–strain for stretched filaments. *Journal of Non-Newtonian Fluid Mechanics*. 2008;151(1-3):38-58.

22. Yao M, Spiegelberg SH, McKinley GH. Dynamics of weakly strain-hardening fluids in filament stretching devices. *Journal of Non-Newtonian Fluid Mechanics*. 2000;89(1-2):1-43.

23. Matallah H, Banaai MJ, Sujatha KS, Webster MF. Modelling filament stretching flows with strain-hardening models and sub-cell approximations. *Journal of Non-Newtonian Fluid Mechanics*. 2006;134(1-3):77-104.

24. Torres MD, Hallmark B, Wilson DI, Hilliou L. Natural Giesekus fluids: Shear and extensional behavior of food gum solutions in the semidilute regime. *AIChE Journal*. 2014;60(11):3902-3915.

25. Giesekus H. A simple constitutive equation for polymer fluids based on the concept of deformation-dependent tensorial mobility. *Journal of Non-Newtonian Fluid Mechanics*. 1982;11(1-2):69-109.

26. Clasen C, Eggers J, Fontelos MA, Li J, McKinley GH. The beads on a string structure of viscoelastic threads. *Journal of Fluid Mechanics*. 2006;556:283-308.

27. Steffe J. *Rheological Methods in Food Process Engineering*. East Lansing: Freeman Press; 1996.

28. Liang RF, Mackley MR. Rheological characterization of the time and strain dependence for polyisobutylene solutions. *Journal of Non-Newtonian Fluid Mechanics*. 1994;52(3):387-405.

29. Clasen C, Plog JP, Kulicke W-M, et al. How dilute are dilute solutions in extensional flows? *Journal of Rheology*. 2006;50(6):849.

30. Larson RG. *Constitutive Equations for Polymer Melts and Solutions: Butterworths Series in Chemical Engineering*. Elsevier Science; 2013.

31. Kvålseth TO. Cautionary Note about R^2. *The American Statistician*. 1985;39(4):279-285.

32. Fylstra D, Lasdon L, Watson J, Waren A. Design and use of the Microsoft Excel Solver. *Interfaces*. 1998;28(5):29-55.

33. Lasdon L, Waren A, Jain A, Ratner M. Design and testing of a generalized reduced gradient code for nonlinear programming. *ACM Transactions on Mathematical Software*. 1978;4(1):34-50.

34. Frontline Systems Inc. *Frontline Solvers - Reference Guide. Version 2015-R2.* Incline Village, NV; 2015.

35. Schleiniger G. A remark on the Giesekus viscoelastic fluid. *Journal of Rheology*. 1991;35(6):1157.

36. Yoo JY, Choi HC. On the steady simple shear flows of the one-mode Giesekus fluid. *Rheologica Acta*. 1989;28(1):13-24.

37. Tirtaatmadja V, McKinley GH, Cooper-White JJ. Drop formation and breakup of low viscosity elastic fluids: Effects of molecular weight and concentration. *Physics of Fluids*. 2006;18(4):043101.

38. Gauri V, Koelling KW. Extensional rheology of concentrated poly(ethylene oxide) solutions. *Rheologica Acta*. 1997;36(5):555-567.

39. Ramanan V V., Bechtel SE, Gauri V, Koelling KW, Forest MG. Exploiting accurate spinline measurements for elongational material characterization. *Journal of Rheology*. 1997;41(2):283.

40. Stelter M, Brenn G, Yarin AL, Singh RP, Durst F. Validation and application of a novel elongational device for polymer solutions. *Journal of Rheology*. 2000;44:595.

List of Tables

Table 1. Analytical expressions used to describe filament thinning, $D(t)/D_0$.

Constitutive model	Equation	Notes	Key reference
Newtonian	$\frac{D}{D_0} = 1 - \frac{(2X-1)\alpha}{3\eta_0 D_0} t$	The shape factor, *X*, corrects for non-cylindrical filaments[3] .	Entov and Hinch[14], Stelter *et al.*[40]
Upper Convected Maxwell (UCM)	$\frac{D}{D_0} = \exp\left(\frac{-t}{3\lambda}\right)$	Simplest viscoelastic fluid model.	Stelter *et al.*[40]
Giesekus	$(4a-3)\ln\left(\frac{D/D_0 + 2\alpha\lambda a/\eta_0 D_0}{1 + 2\alpha\lambda a/\eta_0 D_0}\right) - \frac{2\eta_0 D_0}{\alpha\lambda}\left(D/D_0 - 1\right) = \frac{t}{\lambda}$	Implicit in *D*, explicit in *t*.	Torres *et al.*[24]
FENE	$\frac{D}{D_0} = \left(\sum_i \left(\frac{g_i D_0}{2\alpha}\right) \exp\left(\frac{-t}{\lambda_i}\right)\right)^{1/3}$	Applies to dilute suspension of non-interacting FENE dumbbells. Multimode model with *i* relaxation times.	Entov and Hinch[14], Anna and McKinley[7]
FENE-P	$\left(\frac{1}{1+E_c(b+3)} - \frac{1}{1+\xi E_c(b+3)}\right) + 3\ln\left(\frac{1+\xi E_c(b+3)}{1+E_c(b+3)}\right) + 4E_c\frac{(b+3)}{(b+2)}(\xi-1) = -\frac{(b+3)^2}{b(b+2)}t'$ where $\xi = \frac{D}{D_0}$; $t' = \frac{t}{\lambda}$; $E_c = \frac{gD_0}{2\alpha}$		Wagner *et al.*[15]

Table 2. Datum parameters for sensitivity study.

a (-)		η_0 (Pa s)		λ (s)		D_0 (mm)	α (N/m)
a_1	a_2	$\eta_{0,1}$	$\eta_{0,2}$	λ_1	λ_2	0.25	0.072
0.020	0.020	10.0	0.050	1.00	0.050		

Table 3. Parameters used to generate idealised experimental data in Figure 9(A) and initial conditions and final parameters for data fit shown in Figure 9(B). D_0 = 0.25 mm and α = 0.072 N/m.

Parameter set	$a \times 10^4$ (-)		η_0 (Pa s)		λ (s)		$\eta_{E,1}$ (Pa s)	$\eta_{E,2}$ (Pa s)	R_1^2 (-)
	a_1	a_2	$\eta_{0,1}$	$\eta_{0,2}$	λ_1	λ_2			
Idealised data	20.0	80.0	1.00	0.100	1.00	0.100	1000	25	
Fit - Initial condition	1.78	1.78	0.209	0.007	0.165	0.021	2350	80	
Fit - Final values	168	0.14	0.209	0.007	0.102	1.00	24.8	999	1.00

Table 4. Parameters obtained by fitting Equation (11) to the PEO extensional data shown in Figure 5(A) and to the pitcher fluid extensional data shown in Figure 5(B). For pitcher fluids, assumed value of α = 0.072 N/m; for PEO, α = 0.063 N/m[37]

Parameter set	$a \times 10^4$ (-)		η_0 (Pa s)		λ (s)		$\eta_{E,1}$ (Pa s)	$\eta_{E,2}$ (Pa s)	D_0 (mm)	R_1^2 (-)
	a_1	a_2	$\eta_{0,1}$	$\eta_{0,2}$	λ_1	λ_2				
6 wt% 900k PEO	5.47	7.29	0.230	0.012	5.00*	0.53	840	33.5	0.336	0.988
Pitcher fluid – 3 days	2.60	66.1	0.290	0.027	0.495	0.350	2230	8.12	0.248	0.994
Pitcher fluid – 7 days	1.75	36.1	0.320	0.025	0.284	0.207	3650§	13.6§	0.218	0.994

*5 s was set as the upper constraint on relaxation time.

§ See discussion in text concerning these values

Figure captions

Figure 1. Schematic diagram of traditional, twin-piston, capillary break-up rheometry. A cylindrical sample is loaded between two circular pistons (a). The pistons move apart an equal distance (b) forming a cylindrical filament having an initial mid-point diameter D_0 (c). The filament then thins under the action of surface tension (d)

Figure 2. Photograph of the portable extensional rheometer, Seymour.

Figure 3. Schematic diagram of Seymour's operation. A cylindrical sample is loaded between two circular pistons (a). The top piston then moves away from the bottom piston (b) forming a filament having an initial diameter D_0 (c). The filament then thins under the action of surface tension (d).

Figure 4. Plot of normalised filament diameter as a function of time for Newtonian (α = 0.072 N/m, η_0 = 80 mPas, X = 1), Upper Convected Maxwell (λ = 0.07 s) and Giesekus (α = 0.072 N/m, a = 0.005, η_0 = 1 Pa s, λ = 1 s) models (see Table 1). In all cases D_0 = 0.26 mm and $\boldsymbol{D/D_0 = 1}$ represents the start of surface tension driven filament thinning.

Figure 5. Plot of normalised filament diameter as a function of time for (A) a 6 wt% solution of 900,000 molecular weight PEO in deionised water; and (B) fluid extracted from a pitcher of *N. Rafflesiana* over the course of 7 days. Open circles in (B) represent a newly-opened pitcher (day 0), open triangles the same pitcher 3 days later and crosses the same pitcher at 7 days old. Data have been decimated for clarity after 0.1 s

Figure 6. Plot of normalised filament diameter as a function of non-dimensional time predicted by Equation (11) showing the effect of systematic variation of the rheological parameters governing the short timescale relaxation mode.

Figure 7. Plot of normalised filament diameter as a function of non-dimensional time predicted by Equation (11) showing the effect of systematic variation of the rheological parameters governing the long timescale relaxation mode. The datum is the same as that shown in Figure 6.

Figure 8. Loci of points corresponding to the numerical solution of Equation (11) using parameters given in Table 2 (dotted black line) and the analytical solution of Equation **(26)**, using parameters given in Table 2 with $\boldsymbol{D_H/D_0 = 0.265}$ and $\boldsymbol{t_H/\lambda_1 = 0.031}$, that corresponds to vanishing short mode axial extra stress (solid grey line).

Figure 9. (A) Illustration of fitting the Newtonian and UCM expressions in Table 1 to idealised experimental data generated using Equation (11), using parameters given in row 1 of Table 3, yielding initial estimates of $\eta_{0,1}$, $\eta_{0,2}$ and λ_1 and λ_2 respectively, given in row 2 of Table 3. (B) Loci of points (dashed line) represent best fit of Equation (11) to idealised data (open data points). Final parameters given in row 3 of Table 3.

Figure 10. (A) Plot of normalised filament diameter as a function of time for a 6 wt% solution of 900,000 molecular weight PEO in deionised water. Open circles represent experimental data and the loci of points show the prediction of Equation (11) using the parameters in Table 4. (B) Plot of normalised filament diameter as a function of time for fluid extracted from a pitcher of *N. Rafflesiana* over the course of 7 days. Inset plots the data near filament break-up on linear axes. Open triangles represent a 3-day old pitcher and crosses the same pitcher at 7 days old. Loci of points represent the prediction of Equation (11) with parameters given in Table 4. Experimental data have been decimated for clarity and $\boldsymbol{D/D_0 = 1}$ represents the start of surface tension driven filament thinning.

List of Figures

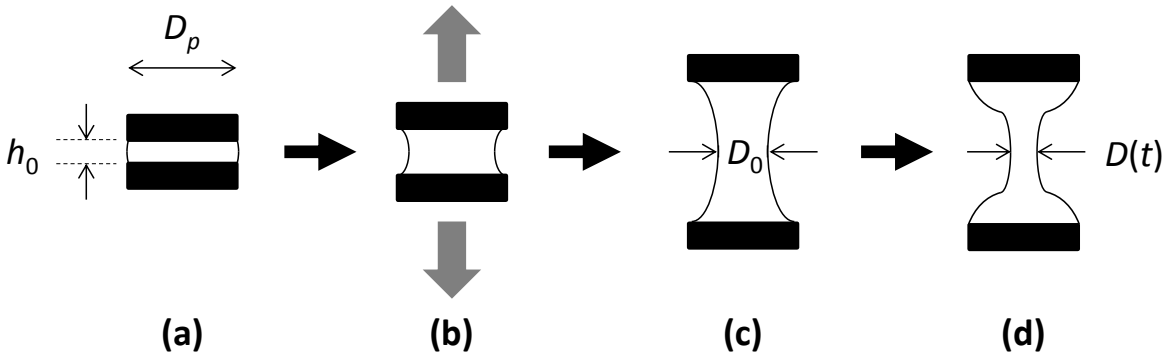

Figure 1. Schematic diagram of traditional, twin-piston, capillary break-up rheometry. A cylindrical sample is loaded between two circular pistons (a). The pistons move apart an equal distance (b) forming a cylindrical filament having an initial mid-point diameter D_0 (c). The filament then thins under the action of surface tension (d), with mid-filament diameter $D(t)$

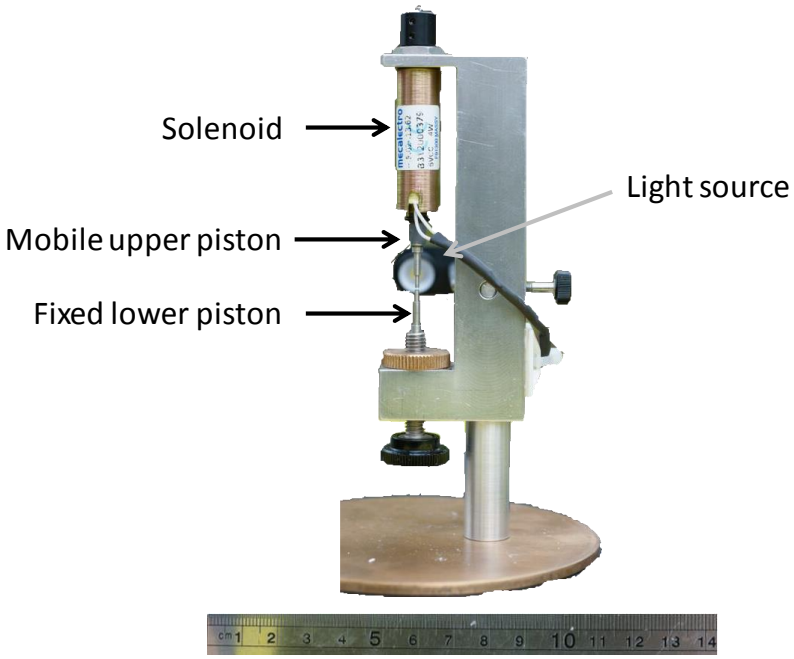

Figure 2. Photograph of the portable extensional rheometer, Seymour.

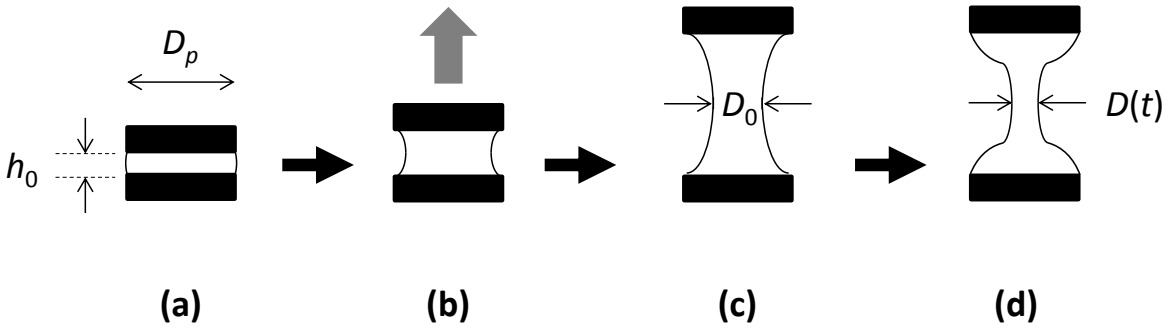

Figure 3. Schematic diagram of Seymour's operation. A cylindrical sample is loaded between two circular pistons (a). The top piston then moves away from the bottom piston (b) forming a filament having an initial diameter D_0 (c). The filament then thins under the action of surface tension (d).

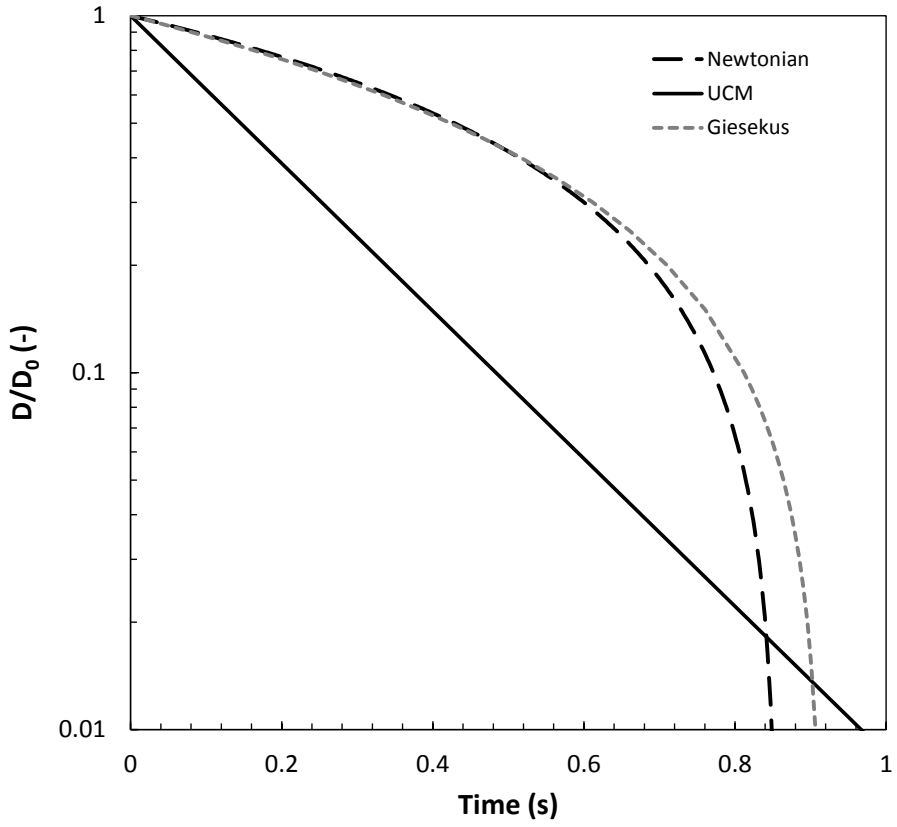

Figure 4. Plot of normalised filament diameter as a function of time for Newtonian (α = 0.072 N/m, η_0 = 80 mPas, X = 1), Upper Convected Maxwell (λ = 0.07 s) and Giesekus (α = 0.072 N/m, a = 0.005, η_0 = 1 Pa s, λ = 1 s) models (see Table 1). In all cases D_0 = 0.26 mm and $D/D_0 = 1$ represents the start of surface tension driven filament thinning.

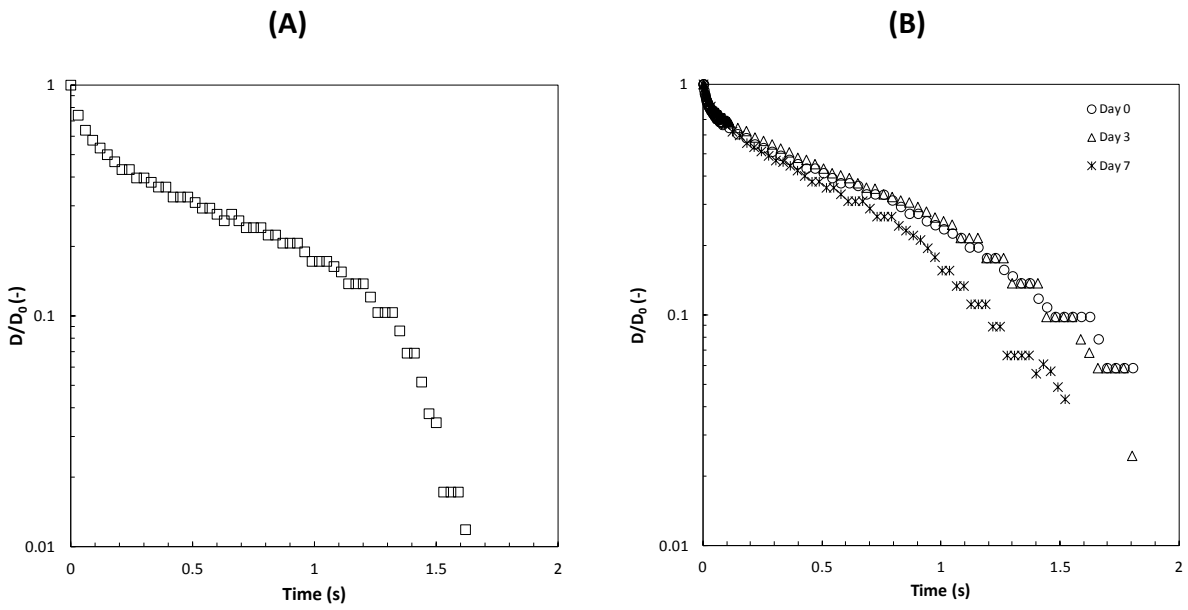

Figure 5. Plot of normalised filament diameter as a function of time for (A) a 6 wt% solution of 900,000 molecular weight PEO in deionised water; and (B) fluid extracted from a pitcher of *N. Rafflesiana* over the course of 7 days. Open circles in (B) represent a newly-opened pitcher (day 0), open triangles the same pitcher 3 days later and crosses the same pitcher at 7 days old. Data have been decimated for clarity after 0.1 s and $D/D_0 = 1$ represents the start of surface tension driven filament thinning.

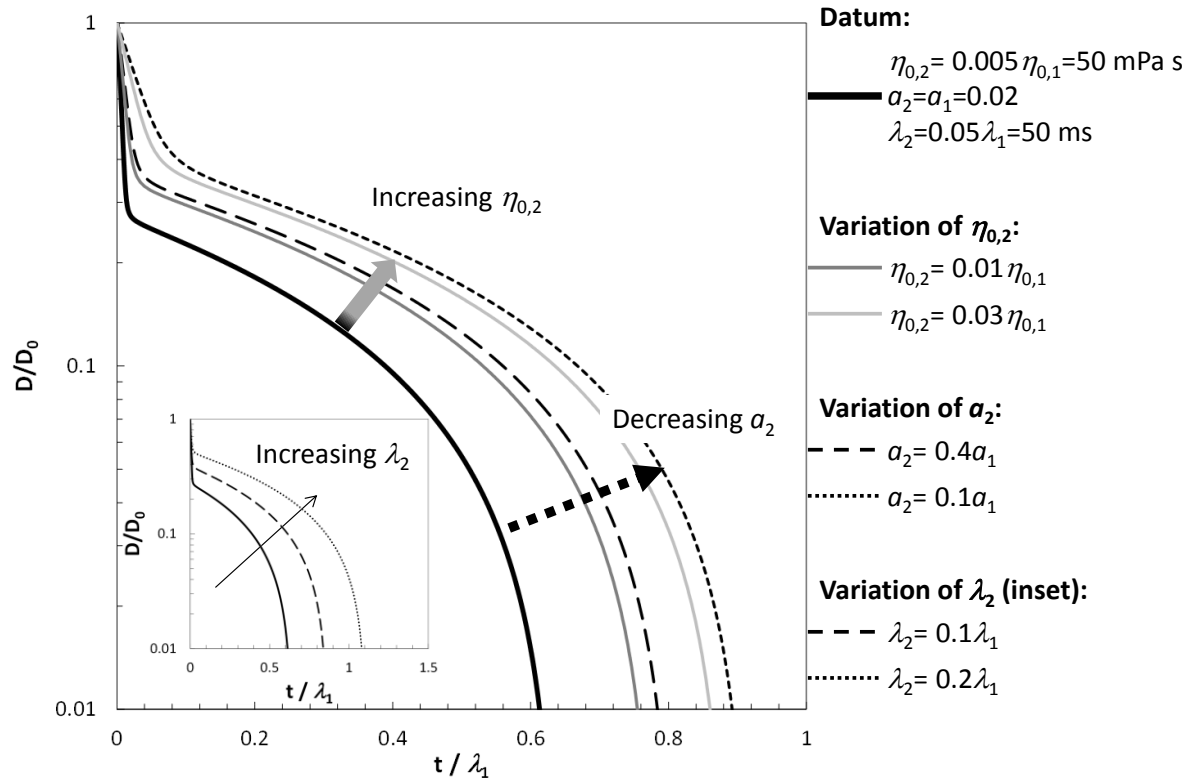

Figure 6. Plot of normalised filament diameter as a function of non-dimensional time predicted by Equation (11) showing the effect of systematic variation of the rheological parameters governing the short timescale relaxation mode.

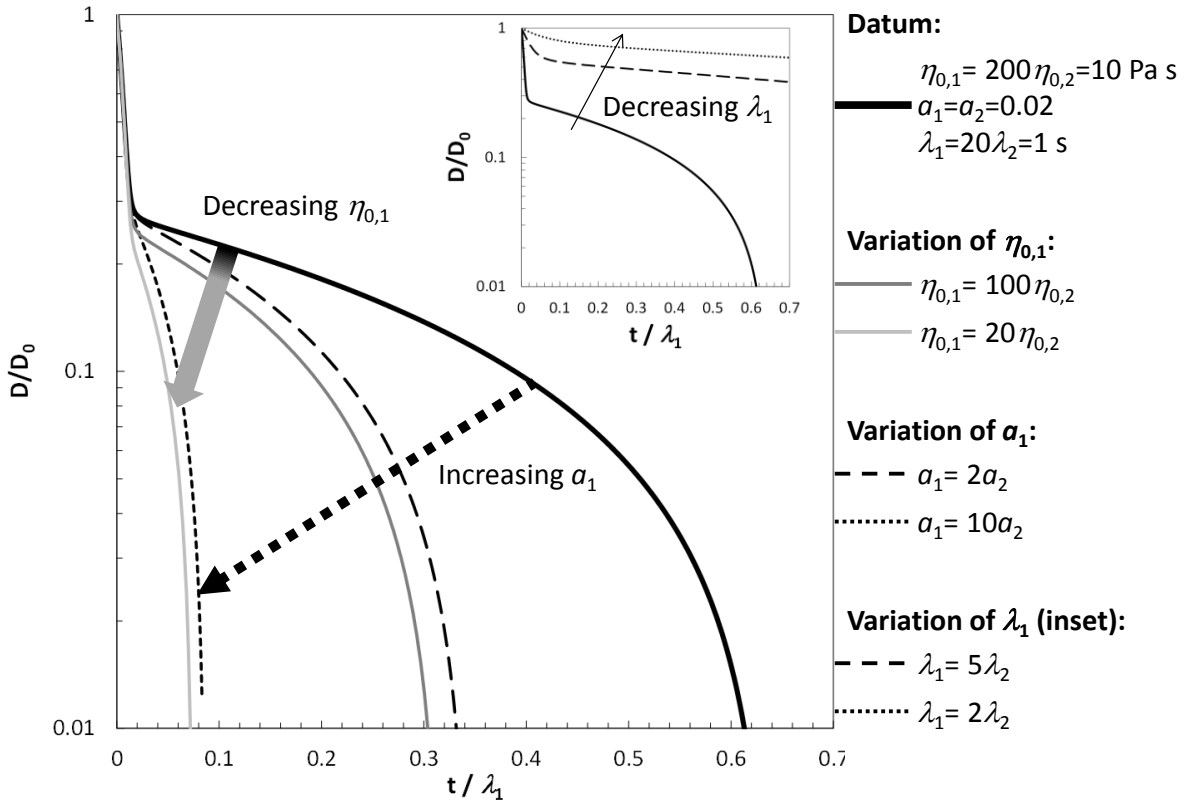

Figure 7. Plot of normalised filament diameter as a function of non-dimensional time predicted by Equation (11) showing the effect of systematic variation of the rheological parameters governing the long timescale relaxation mode. The datum is the same as that shown in Figure 6.

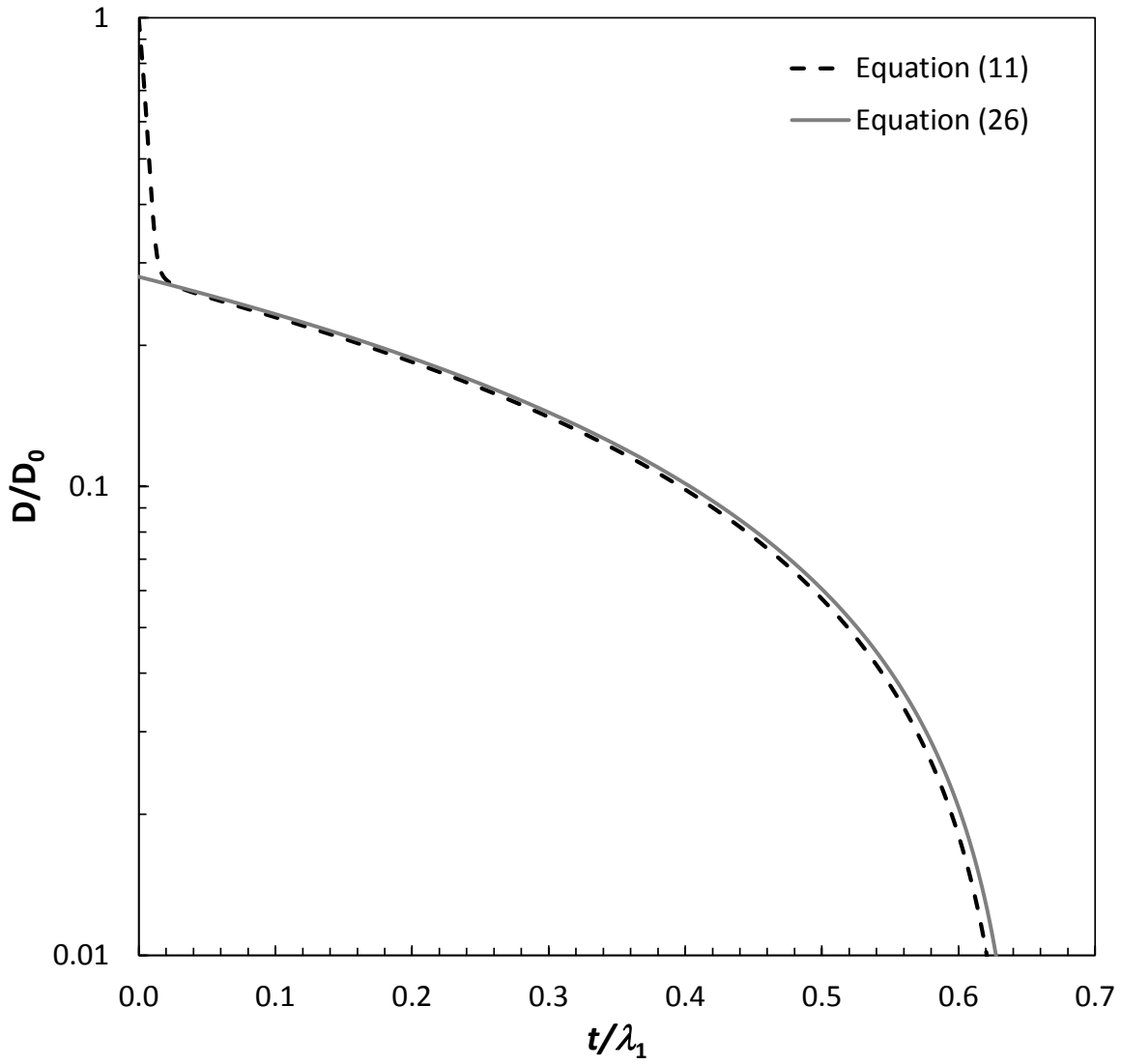

Figure 8. Loci of points corresponding to the numerical solution of Equation (11) using parameters given in Table 2 (dotted black line) and the analytical solution of Equation (26), using parameters given in Table 2 with $^{D_H}/_{D_0} = 0.265$ and $^{t_H}/_{\lambda_1} = 0.031$, that corresponds to vanishing short mode axial extra stress (solid grey line).

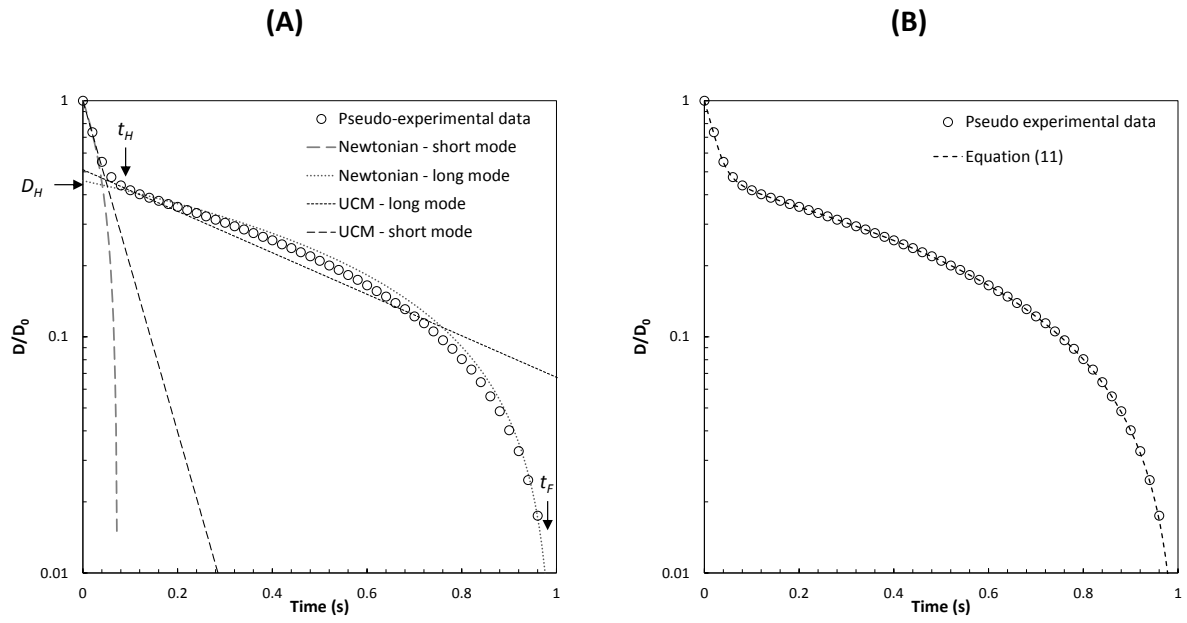

Figure 9. (A) Illustration of fitting the Newtonian and UCM expressions in Table 1 to idealised experimental data generated using Equation (11), using parameters given in row 1 of Table 3, yielding initial estimates of $\eta_{0,1}$, $\eta_{0,2}$ and λ_1 and λ_2 respectively, given in row 2 of Table 3. (B) Loci of points (dashed line) represent best fit of Equation (11) to idealised data (open data points). Final parameters given in row 3 of Table 3.

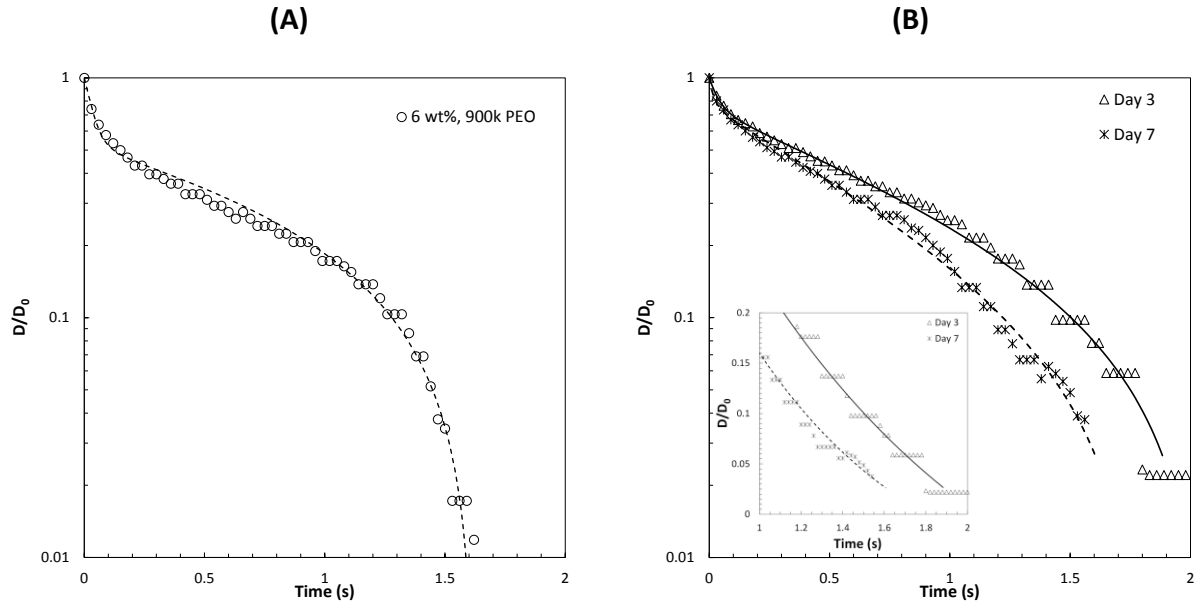

Figure 10. (A) Plot of normalised filament diameter as a function of time for a 6 wt% solution of 900,000 molecular weight PEO in deionised water. Open circles represent experimental data and the loci of points show the prediction of Equation (11) using the parameters in Table 4. (B) Plot of normalised filament diameter as a function of time for fluid extracted from a pitcher of *N. Rafflesiana* over the course of 7 days. Inset plots the data near filament break-up on linear axes. Open triangles represent a 3-day old pitcher and crosses the same pitcher at 7 days old. Loci of points represent the prediction of Equation (11) with parameters given in Table 4. Experimental data have been decimated for clarity and $D/D_0 = 1$ represents the start of surface tension driven filament thinning.